iScience

CellPress
OPEN ACCESS

Article

Extended Metabolic Biosensor Design for Dynamic Pathway Regulation of Cell Factories

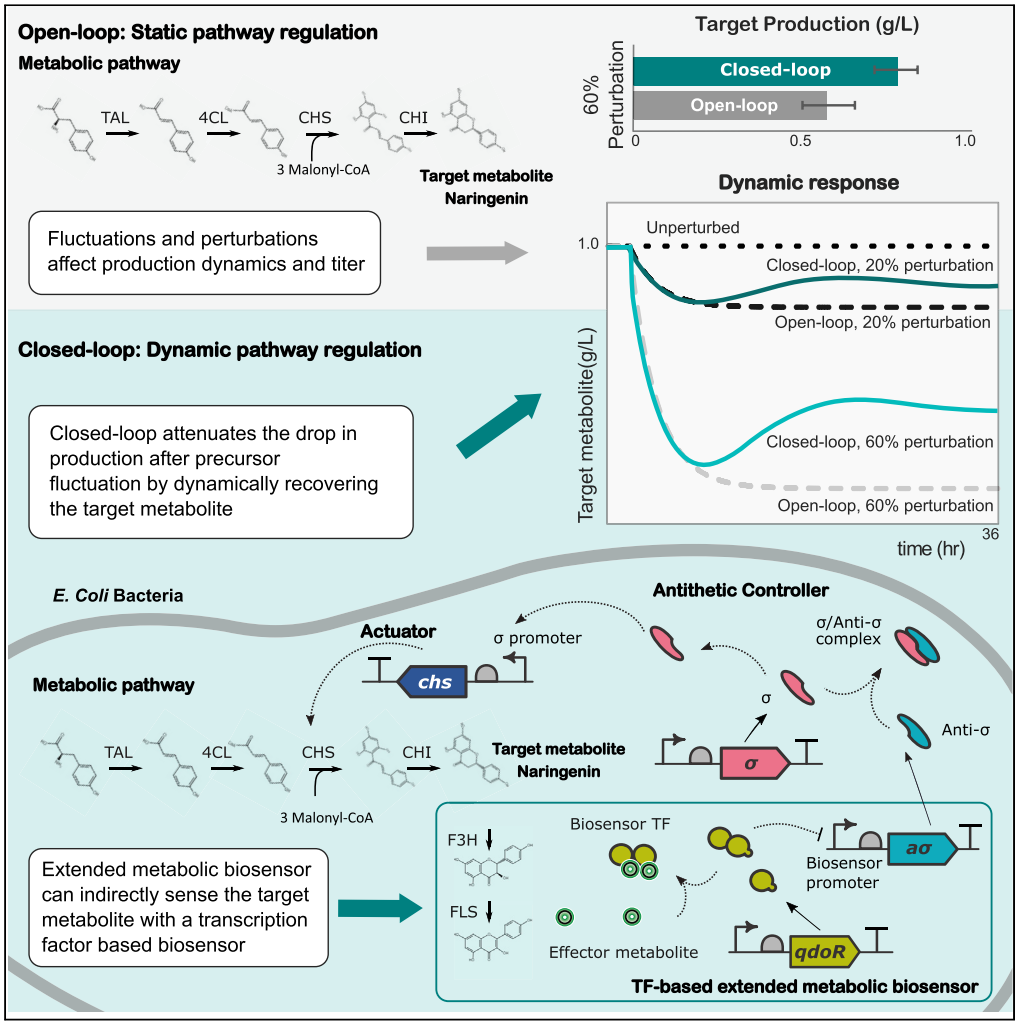

Yadira Boada, Alejandro Vignoni, Jesús Picó, Pablo Carbonell

pjcarbon@isa.upv.es

HIGHLIGHTS

Fluctuations and perturbations affect dynamics and titers in cell factories

Extended metabolic biosensors expand product sensing and enable pathway regulation

Closed-loop pathway regulation provides robustness to cell factory production

A closed-loop regulated flavonoid production pathway shows robust dynamic response

Boada et al., iScience 23, 101305
July 24, 2020
https://doi.org/10.1016/j.isci.2020.101305

iScience

CellPress
OPEN ACCESS

Article

Extended Metabolic Biosensor Design for Dynamic Pathway Regulation of Cell Factories

Yadira Boada,[1,2] Alejandro Vignoni,[1] Jesús Picó,[1] and Pablo Carbonell[1,3,*]

SUMMARY

Transcription factor-based biosensors naturally occur in metabolic pathways to maintain cell growth and to provide a robust response to environmental fluctuations. Extended metabolic biosensors, i.e., the cascading of a bio-conversion pathway and a transcription factor (TF) responsive to the downstream effector metabolite, provide sensing capabilities beyond natural effectors for implementing context-aware synthetic genetic circuits and bio-observers. However, the engineering of such multi-step circuits is challenged by stability and robustness issues. In order to streamline the design of TF-based biosensors in metabolic pathways, here we investigate the response of a genetic circuit combining a TF-based extended metabolic biosensor with an antithetic integral circuit, a feedback controller that achieves robustness against environmental fluctuations. The dynamic response of an extended biosensor-based regulated flavonoid pathway is analyzed in order to address the issues of biosensor tuning of the regulated pathway under industrial biomanufacturing operating constraints.

INTRODUCTION

Natural cells maintain robust growth and withstand environmental fluctuations by dynamically adjusting cellular metabolism through complex regulatory networks (Liu et al., 2018). Since nature has optimized metabolite production for its needs, these specific optimal solutions are usually not compatible with industry-level overproduction demands. Major improvements in yield, titer, and productivity of engineered metabolic pathways can be accomplished by balancing pathway gene expression (Liu et al., 2018). The objective is to increase production of the target product through reducing potential flux imbalances in the host organism. This is mainly accomplished by eliminating the production of excessive intermediate metabolites and precursors leading to efficient conversion of intermediates, substrates, and co-factors to desired products. There exist several metabolic pathway-balancing approaches that optimize gene expression and flux distribution based on *in silico* predictions provided by static constraint-based metabolic genome-scale models (Purdy and Reed, 2017), using regulatory elements (DNA copy number, promoter and ribosome binding site [RBS] engineering) (Nielsen et al., 2016), synthetic scaffolds, compartmentalization, and flux diversion (silencing, knockouts, alternative carbon sources) (Chae et al., 2017). These pathway regulation strategies optimizing for a particular condition are static, so they are unable to respond to growth and environmental changes that occur in a bioreactor setup (Shi et al., 2018; Wehrs et al., 2019). Moreover, these static control systems may not be suitable when piecing together a complicated pathway with biosynthetic modules with mismatched input/output levels or when there is a need to minimize the accumulation of potentially toxic intermediates (Shi et al., 2018).

Dynamic balancing addresses the robustness pitfalls of static control through the application of feedback and feedforward regulation. This makes it possible to attain higher titers as compared with static regulation (Stevens and Carothers, 2015). However, it is not until recent years that metabolic engineers have used dynamic regulation to redirect endogenous flux toward product formation, balance the production and consumption rates of key intermediates, and suppress production of toxic intermediates in the fermentation (Doong et al., 2018). The main reason is that, in order to implement a dynamic regulation strategy, biosensors are needed. Indeed, a dynamic regulation system consists of a sensing component, which can detect the metabolite of interest or physiological state (e.g., growth, stress signals), and a regulator component, which converts the sensor signal into a transcriptional signal, often resulting in the upregulation or downregulation of a key pathway gene (Paepe et al., 2018; Huyett et al., 2018; Liu and Zhang, 2018).

[1]Synthetic Biology and Biosystems Control Lab, I.U. de Automática e Informática Industrial (ai2), Universitat Politècnica de València, Camí de Vera S/N, 46022 Valencia, Spain

[2]Centro Universitario EDEM, Escuela de Empresarios, Muelle de la Aduana s/n, La Marina de València, 46024 Valencia, Spain

[3]Lead Contact

*Correspondence: pjcarbon@isa.upv.es

https://doi.org/10.1016/j.isci.2020.101305

Despite a growing number of success stories, engineering dynamic control remains extremely challenging (Chen and Liu, 2018; Gao et al., 2019). Among these challenges, one can count cell resource allocation, microorganism population heterogeneity, and fluctuating industry-scale bioreactor environment. Moreover, the performance specifications for synthetic gene circuits and components change significantly with variations in parameters such as temperature, host organism, growth media formulation, and position of the genes in the genome (Segall-Shapiro et al., 2018). To address these challenges, model-based design relying on the principles of control engineering can provide a powerful formalism to engineer dynamic control circuits. These, together with the tools of synthetic biology, can lead to robust and efficient microbial production at industrial levels (Liu et al., 2018; Segall-Shapiro et al., 2018; Hsiao et al., 2018; Shopera et al., 2017; Boada et al., 2017a, 2017b).

Biosensor mechanisms that translate information about a chemical signal (the concentration of a natural product) into a measurable output are being increasingly used in engineering and synthetic biology (Johnson et al., 2017; Shi et al., 2018; D'Ambrosio and Jensen, 2017). Intracellular biosensors can be broadly grouped into three categories, RNA switchers (aptamers) (McKeague et al., 2016), reporter-proteins leading to signal generation (Agrawal et al., 2020), and transcription factors (TF) leading to transcriptional regulation (Mahr and Frunzke, 2015), on the basis of their biomolecular make-up and mechanism. TF-based biosensors present advantages in terms of specificity and sensitivity (Lin et al., 2017). However, the use of biosensors in synthetic circuits to control gene expression is in its beginnings, as the tunability of the biosensor is essential for dynamic control systems to appropriately function in industrial conditions (Liu et al., 2018; Wang et al., 2019). Only recently, libraries of TF-based biosensors have been created by varying regulatory elements such as RBS (Paepe et al., 2018). Also, the biosensor dynamic range and thresholds can nowadays be modified through directed evolution (Snoek et al., 2019) or with the use of model-based design for the constraints of dose-response curves (Mannan et al., 2017). However, reported chemicals that can be detected by TF-based biosensors are generally focused on some specific classes of compounds such as amino acids and do not cover the entire range of nature's chemical diversity. SensiPath (Delépine et al., 2016) has been recently introduced to develop extended TF-based biosensors through metabolic pathways, thus expanding the observable chemical space spanned by biosensors.

Extended metabolic biosensor-based circuits considerably enlarge the ability of sensing target molecules for pathway screening and regulation. Such type of genetic circuits can be computationally designed through an *in silico* screening of the extended metabolic space (Carbonell et al., 2014; Delépine et al., 2016). As the number of characterized transcription factors that are responsive to effector molecules is constantly increasing, the number of possible ways of setting up a genetic circuit encoding an extended metabolic biosensor for the desired target increases as well. Currently, the number of known small-molecule chemical effectors for transcription factors is close to 750 (Koch et al., 2018) providing a large design space that can be explored in order to select the optimal biosensor circuit depending on the objectives. Given the set of reachable metabolites, i.e., chemicals that can be produced through enzymatic transformations, and the set of effector metabolites that can induce or modulate the response of a transcription factor, we define the set of biosensor circuits as all possible biosynthetic metabolic pathways that can convert the desired target into one of the metabolites within the effectors set.

In order to streamline the design and use of TF-based biosensors for dynamic regulation of metabolic pathways, in this study we aimed at introducing an extended metabolic biosensor-based antithetic control for regulating the heterologous pathway of the flavonoid naringenin production in the *Escherichia coli* host. We chose the naringenin pathway as our case study because of the availability of both direct and indirect TF-based biosensors for intermediates and derivatives involved in the production of this class of compounds of industrial biomanufacturing interest. Flavonoids are an important subclass of phenylpropanoids, a major family of plant natural products with applications as food supplements, antioxidants, aroma and flavoring agents, pharmacological drugs, insecticides, and dyes. Clear market opportunities exist for flavonoids with enhanced bioavailability and bioactivity profiles used as flavors and bioactive compounds for nutraceutical applications among others. The flavonoid compound naringenin is predominantly found in grapefruits and oranges and has been reported to have many pharmacological properties, including anti-dyslipidemic, anti-obesity and anti-diabetic, and anti-fibrotic (Liu et al., 2008; Rahigude et al., 2012; Zygmunt et al., 2010). It also has a central place in the biosynthesis of all flavonoids, as naringenin plays an important role as backbone scaffold that can be further derivatized. Downstream pathways may add biochemical groups on it. These molecular modifications (derivatizations) are responsible for functionalization and diversification of end products in the broad families of flavonoids.

Although microbial fermentation of naringenin has been achieved, current titers do not render its microbial production economically feasible. Current maximum reported titers for production of naringenin in industrial hosts are close to 200 mg L^{-1} (Zhou et al., 2019). However, industrial levels above 1 g L^{-1} might be possible to reach through further optimization toward the maximum theoretical yield. Notably, Juminaga et al. (2011) optimized the production of the L-tyrosine precursor in *E. coli*, achieving a yield of 0.44 g *L*-tyrosine/g glucose, which was determined to correspond to 80% of the maximum theoretical yield. The obtained yield allowed the production of 2.2 g L^{-1} of *L*-tyrosine in 48 h. Moreover, a titer of 474 mg L^{-1} of naringenin has been reported when feeding *p*-coumarate by host optimization (Xu et al., 2011). Therefore, we expect that the titers can go still up, especially because of the high efficiency of the conversion of *L*-tyrosine into *p*-coumarate, and should be able to reach at least 0.4 g naringenin/g glucose and a titer of 800 mg L^{-1} in 48 h in a fermenter, with still some room for further optimization through additional strain optimization, chromosome integration, and process optimization. Besides the increase in the amount of molecules per cell, the final titers of naringenin in *E. coli* can also be significantly increased by using high-density culture bioreactors, which can reach cell concentrations above 100 OD (Choi et al., 2006).

The naringenin pathway consists of four enzymatic steps from the *L*-tyrosine precursor. The third step, catalyzed by naringenin chalcone synthase (CHS) requires malonyl-CoA, an essential metabolite that is used in fatty acid production and plays an important role in cell metabolism. Intracellular concentrations of malonyl-CoA are typically low (4–40 μM in *E. coli*) (Johnson et al., 2017; Xu et al., 2014). Moreover, its concentration is subject to fluctuations caused by cell environmental heterogeneities. Several strategies have been used in order to channel the malonyl-CoA flux into the desired production pathway, including overexpression of the enzyme that synthetizes it or down-regulation (Yang et al., 2015). However, accumulation of malonyl-CoA leads to growth inhibition. Therefore, just-in-time dynamic production of malonyl-CoA appears as a desired goal.

Dynamic redistribution of cellular resources and optimal control of pathway expression offer alternative strategies for engineering metabolic pathways with high productivity and yield. In Xu et al. (2014) the FapR TF-based malonyl-CoA biosensor (Johnson et al., 2017) is used to design a metabolic switch that enables dynamic regulation of both the malonyl-CoA source pathway and its sink pathway in order to dynamically regulate malonyl-CoA concentration. The engineered strain improved fatty acids production as it reached a better trade-off between cell growth and heterologous pathway expression. As an alternative, Dinh et al. (2020) obtained a 60% titer increase in the production of naringenin by controlling the composition of a co-culture using a quorum sensing-based growth-regulation circuit.

Here, we will use a different approach where a naringenin biosensor is used to establish a feedback control system that will regulate the levels of expression of the naringenin chalcone synthase enzyme in order to provide a robust response to the fluctuations in malonyl-CoA availability and maximize the production of the naringenin target. Notably, our strategy, as depicted in Figure 1, will consist of initially establishing a baseline production pathway for naringenin and to use an extended biosensor-based feedback control system to regulate naringenin production around its nominal level while coping with fluctuations in the malonyl-CoA availability.

RESULTS

Response of the Naringenin TF-based Extended Metabolic Biosensor

The FdeR transcription factor is responsive to naringenin and has been used as a biosensor for high-throughput screening. However, its dynamic range is 0.001–0.15 mM, i.e., it saturates around 40 mg L^{-1}, which means that, even if that biosensor could be used during the prototyping stage to implement pathway regulation, its use for feedback regulation is not viable at the desired industrial levels. Therefore, it is necessary to search for a transcription factor-based flavonoid biosensor, such as those reported in the literature (Cheng et al., 2018), that performs an indirect measurement allowing tuning of the dynamic range.

A promising case is a biosensor circuit based on the transcription factor QdoR for kaempferol and quercetin, two flavonols that can be derived from naringenin in two and three conversion steps, respectively. This transcription factor, with a similar dynamic range than the one for naringenin, can provide an extended metabolic biosensor-based solution for naringenin high-producer strains. Conversion ratios for quercetin of 13:1 in *E. coli* (Leonard et al., 2006) and of 100:3 in yeast (Trantas et al., 2009) have been reported; therefore, it is possible to extend the net dynamic range for naringenin above 1 g L^{-1} even if the use of

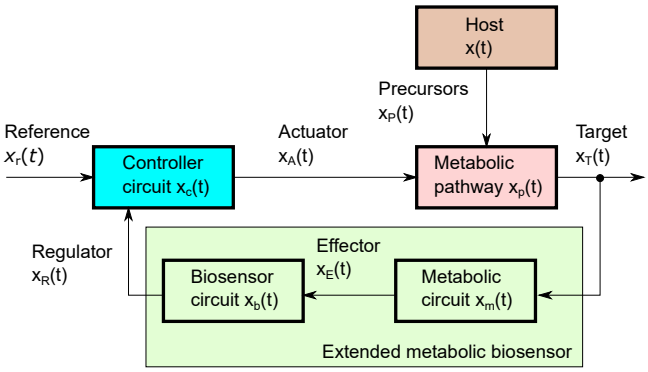

Figure 1. Schematic Diagram of the Proposed Strategy

A target-producer metabolic pathway is expressed in the host, where the fluctuating availability of precursors $x_P(t)$ act as perturbations that eventually affect the target metabolite production $x_T(t)$. This is sensed using an extended metabolic biosensor device comprising a metabolic pathway that converts the target into an effector metabolite $x_E(t)$ and an associated transcription factor-based biosensor that provides the regulation signal $x_R(t)$. This one is fed back to a gene regulatory circuit that expresses the actuator signal $x_A(t)$ driving the target metabolite toward the specified set-point $x_r(t)$. In our case, the actuator signal $x_A(t)$ consists of a parallel expression system for the limiting precursor $x_P(t)$.

a QdoR-based biosensor compared with a FdeR-based one would introduce some additional challenges. One challenge of this approach is that, in order to produce kaempferol or quercetin, naringenin needs to be consumed and some of the intermediates might accumulate at high concentrations. However, a recent study has shown that, through appropriate selection of the enzymes in the pathway, it is possible to tune the levels of accumulation of each intermediate (Rodriguez et al., 2017). In that study, production for each intermediate was optimized by trying to reduce accumulation of the other compounds. For the biosensor case, the goal would be to keep naringenin at high levels with a low conversion ratio to kaempferol, and a minimal accumulation of the intermediate dihydrokaempferol.

The TF-based extended metabolic biosensor proposed in this work, depicted in Figure 2, uses the downstream metabolite kaempferol as proxy of naringenin. Kaempferol in turn captures the QdoR transcription factor, which represses the expression of the anti-σ molecule by means of the qdoR-Pqdol promoter region (Siedler et al., 2014). In this way, increasing values of naringenin will produce increasing values of anti$-\sigma$. Thus, the naringenin TF-based extended biosensor starting from naringenin generates the sensor input signal, and the sensor output signal coming from anti$-\sigma$ is fed back to the controller. The resulting extended biosensor was modeled as described in Transparent Methods section in the Supplemental Information.

Figure 3 shows the dynamic range of the biosensor according to its dose-response curve. For instance, to sense 1 g L^{-1} of naringenin, the extended biosensor needs to convert only 5 μg L^{-1} of kaempferol. This means that the extended biosensor has a very low gain, allowing the biosensor promoter to work in the non-saturated region while responding to changes of naringenin concentration in the g L^{-1} range. To that end, the metabolic part of the extended biosensor had to be tuned in such a way that it produces very low amounts of kaempferol for large amounts of naringenin. This can be achieved, for instance, by tuning for a very low affinity to the substrate. This is particularly relevant for the first enzyme of the biosensor. In a similar fashion, the rest of the enzymes of the extended pathway need to show low efficiency. Based on such designated enzyme configuration, parameters in the system were adjusted as described in Metabolic pathway and Table S1 in the Supplemental Information, and the corresponding dynamic response of the biosensor was analyzed. The insets of Figure 3 show the time response of the naringenin extended metabolic biosensor. Figure 3C shows the time response of kaempferol to a sudden change in the naringenin concentration, whereas Figure 3D shows the time response of anti-σ, the sensor output signal. As expected, similar dynamics between a change in the naringenin concentration and the response to that change were found in both concentrations of kaempferol and anti-σ. The apparent delay introduced by the slow dynamics can be mainly attributed to the dilution of kaempferol due to cell growth. Interestingly, as detailed later, the integral antithetic controller is able to provide the desired robust response, despite this extra dynamics in the loop. Notice also that the low gain of the biosensor contributes to reduce the metabolic burden it introduces.

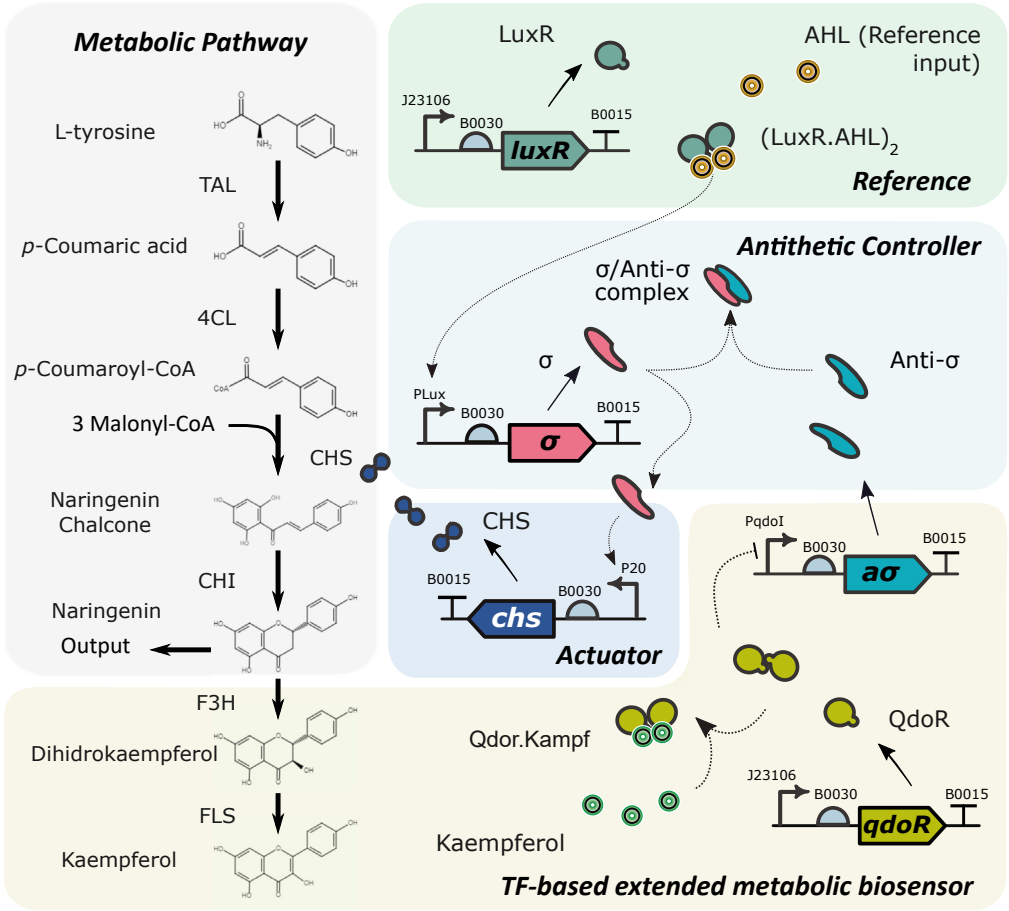

Figure 2. Naringenin Pathway, Antithetic Controller and TF-Based Extended Metabolic Biosensor

Production of the naringenin target is proxied by a metabolic circuit through the downstream metabolite kaempferol, which is sensed by the QdoR transcription factor and feeds back to an antithetic controller. The controller is activated upstream by the external AHL inducer, and its actuating signal overdrives the expression of the CHS enzyme in the pathway, in order to compensate for malonyl-CoA depletion.

Response of the Antithetic Integral Feedback Regulator

To adopt the use of extended metabolic biosensor circuits in pathway regulation, important effects may impact their performance; therefore, they need to be considered. Such effects appear because of the delays and nonlinearities introduced by the metabolic circuit. For screening applications, they can often be compensated through calibration of the biosensor. In pathway dynamic regulation nevertheless, the effects can have a strong impact on the performance of the pathway and even bring it to unstable behavior (Hsiao et al., 2018). Hence, it is necessary to establish a control strategy for counteracting the inherent uncertainties of the response for a given design and to determine the conditions and ranges that must be verified by the extended metabolic biosensor parameters in order to guarantee a stable and robust response.

To that end, integral feedback control appears as a promising solution for robust output regulation against perturbations. The antithetic feedback control is a type of integral control that has been recently shown to be a universal genetic topology that can achieve robust perfect adaptation (Briat et al., 2016) and has already been considered for regulation of metabolic pathways (Briat and Khammash, 2018). Therefore, the use of a genetic circuit implementing an antithetic integral feedback controller in combination with an extended metabolic biosensor seems a promising genetic system for pathway regulation.

Here we use the antithetic control structure, as depicted in Figure 2, to dynamically express the enzyme CHS catalyzing the conversion from *p*-coumaric acid to naringenin chalcone. The decrease in naringenin

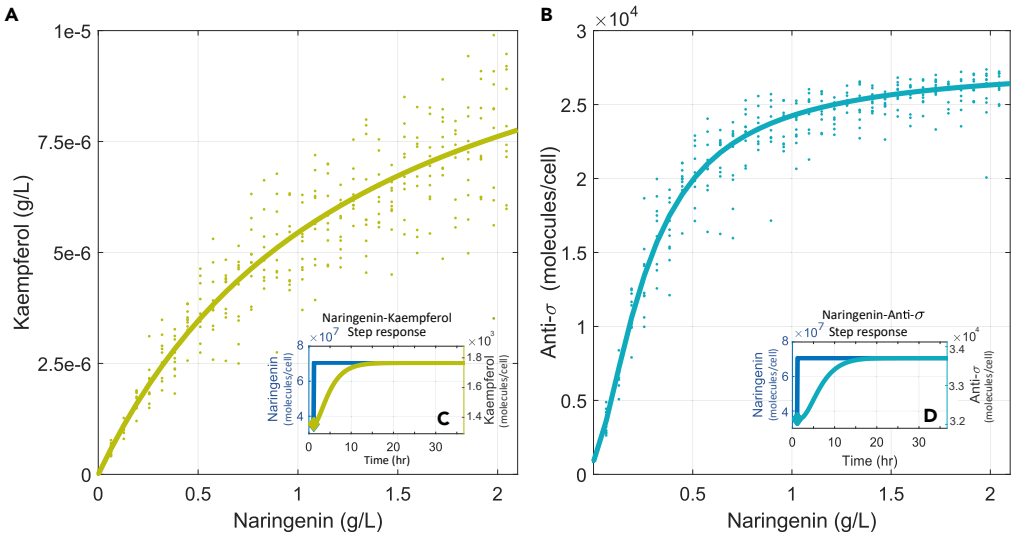

Figure 3. Naringenin TF-based Extended Metabolic Biosensor Dose-Response

(A–D) (A) Naringenin to kaempferol dose-response showing the kaempferol concentration (g L^{-1}) corresponding to a varying range of naringenin production concentrations (g L^{-1}). The inset (C) shows the time response of kaempferol to a sudden step-like change in the concentration of naringenin concentration. (B) TF-based extended metabolic biosensor input-output dose-response. The amount of anti-σ molecules is shown for a varying range of naringenin production levels (g L^{-1}). The inset (D) shows the time response of anti-σ to a sudden step-like change in the concentration of naringenin concentration. In both graphs solid lines are the mean values and dots correspond to the dose-responses under a 15% uncertainty in the biosensor parameters for a plasmid copy number of ten.

implies less amount of both kaempferol and anti−σ factor (Rhodius et al., 2013), and its σ cofactor will no longer be suppressed. Mutual annihilation of the antithetic σ/Anti-σ cofactors provide negative integral feedback (Aoki et al., 2019) to regulate CHS enzyme production under the σ−P20 promoter region. σ Cofactor is activated by the upstream protein LuxR together with the external inducer AHL. Figure 4A illustrates how the CHS enzyme expression is reduced when the σ/Anti-σ negative feedback acts (increasing expression of anti-σ).

Notice that the global amount of CHS in the cell directly modulates the conversion flux from *p*-coumaric acid to naringenin chalcone (see Metabolic pathway in the Supplemental Information). The antithetic controller dynamically provides a variable amount of CHS additional to its basal level of expression. This way the controller compensates for fluctuations affecting the production of naringenin. The dynamics of the controller was modeled as described in section Antithetic controller in the Supplemental Information.

Putting together the previous three dose-response curves one can obtain the dose-response curve (static relationship) of the combined TF-based extended biosensor controller (Figure 4B). This combined dose-response is the complete input-output relationship of the feedback representing how the level of CHS enzyme expression will change upon changes in the naringenin levels. Within the same Figure 4B we also represented in dashed colored lines the production curves that represent the relationship between the production of naringenin and the amount of CHS enzyme for different fixed amounts of malonyl-CoA (for fixed pathway conditions). Note that there is a threshold in the transition above 1 g L^{-1}. As the production curves are calculated for fixed pathway conditions that were selected for nominal levels of 1 g L^{-1}, for higher production values, the rest of the pathways turn to be the limiting process and prevents higher levels of naringenin from being produced.

Once the amount of enzyme is selected, for instance, the amount shown in dotted black line in Figure 4B (representing the open-loop strategy, see Figure S1 in the Supplemental Information for more details, i.e., a fixed amount of enzyme), the intersection of this line with the dashed lines representing the production gives the amount of naringenin produced with that amount of enzyme. Here we see that the open loop strategy results in a decrease of levels of production upon malonyl-CoA reduction. Similarly, the closed-loop equilibrium is the intersection of the closed-loop dose-response curve with the production lines. In

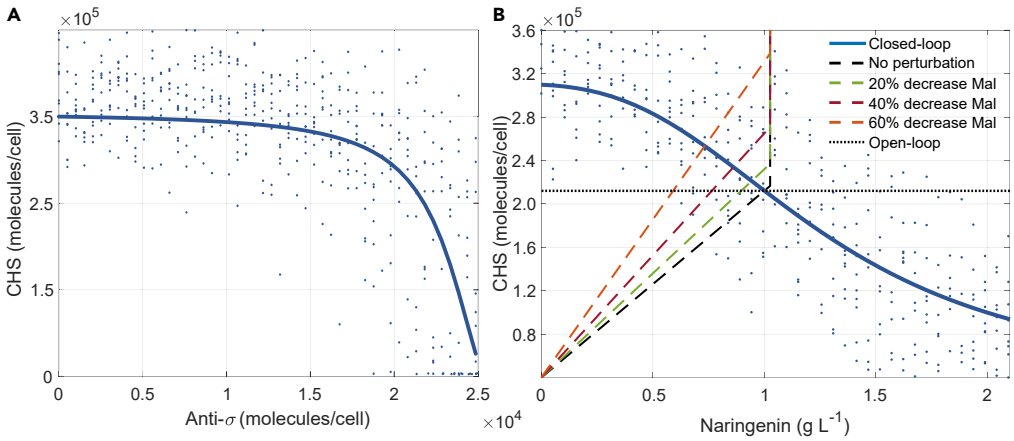

Figure 4. Antithetic Controller Input-Output Dose-Response

(A) The amount of CHS molecules is shown for a varying range of the amount of anti-σ molecules produced by the TF-based extended metabolic biosensor.

(B) Production curve and TF-based extended biosensor/controller combined dose-response. Closed (blue) and open loop (black dotted) dose-responses. Dashed lines represent the relationship between the production of naringenin and the amount of CHS enzyme for different amounts of malonyl-CoA (for fixed pathway conditions). In both graphs solid lines are the mean values and dots correspond to the dose-responses under a 15% uncertainty in the biosensor parameters for a plasmid copy number of ten.

that case, it is possible to see how the closed loop can recover from a reduction in malonyl-CoA availability thanks to the dynamical regulation of the amount of enzyme.

Dynamic Regulation of the Naringenin Pathway

In order to analyze the pathway dynamic regulation and eventually design a robust feedback regulation, the dynamic response of the two enzymatic steps in the extended biosensor in Figure 2 needs to be considered. The kinetics of the involved enzymes, however, have been less studied than of those in the naringenin pathway, and therefore, it would be necessary to assume some level of uncertainty in the parameters associated with the dynamic response of the biosensor. Here, we will assume typical kinetic values for the enzymes in the pathway extracted from the literature (see Methods). Figure 5 depicts the performance assessment of the regulated pathway assuming a model for the system as described in Methods. The output response in closed loop (Figure 5, solid lines), i.e., regulation based on the kaempferol-mediated naringenin biosensor driving an antithetic integral controller (see Figure 2) was compared with the output response in open loop (Figure 5, dashed black line), i.e., without feedback regulation of the CHS concentration (see Figure S1). Moreover, we also compared our strategy with a regulation based on a kaempferol-mediated naringenin biosensor driving a direct feedback controller (Figure 5, dashed blue line), i.e., a repressible promoter (cI regulated promoter) directly driving the expression of CHS enzyme (see Figure S2 and the direct controller model in the Supplemental Information).

The open-loop response results by replacing the P20 promoter that responds to σ (and in turn to naringenin via the biosensor) with a constitutive promoter (see Figure S1 and the open-loop model in the Supplemental Information for more details). This promoter was selected in such way that for the same conditions (same flux of L-tyrosine and malonyl-CoA) it provides the same amount of naringenin as the closed-loop circuit (around 1 g L^{-1}). The direct feedback controller (see Figure S2) involves a repressible promoter (cI regulated promoter) directly driving the expression of the enzyme CHS. In turn, the repressor (cI) is expressed from the same PqdoI promoter of the biosensor. The values of the parameters of this direct controller (see Table S2) were selected to provide the same amount of naringenin as the closed-loop circuit (around 1 g L^{-1}) for the same conditions (same flux of L-tyrosine and malonyl-CoA).

Figure 6 shows the transient responses for different values of malonyl-CoA decrease. The perturbation occurs at time $t = 1$ h. In the regulated case, the levels of production of naringenin were successfully recovered after a transient response of approximately 24–30 h, reaching the end of the experiment at 36 h with a steady production.

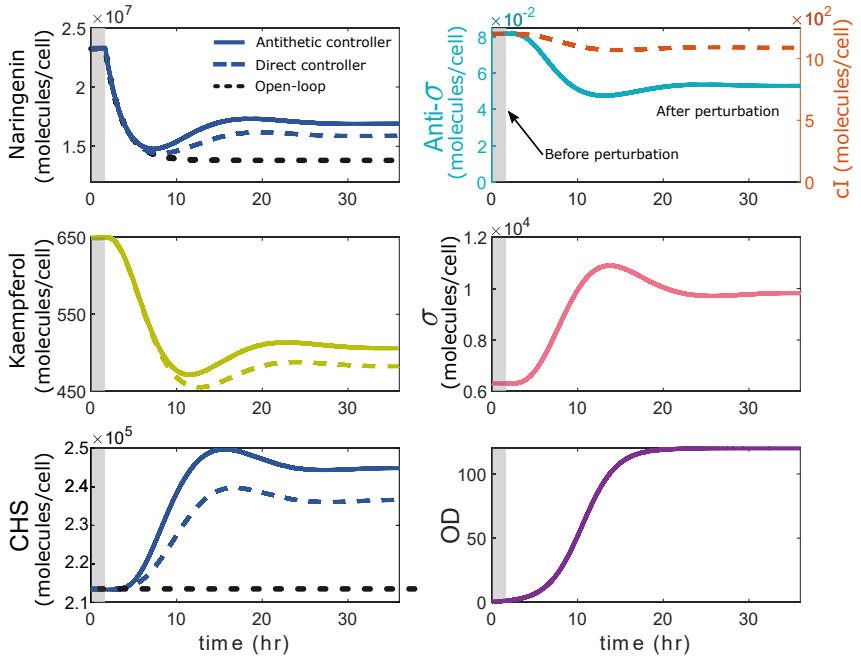

Figure 5. Dynamic Response of the Regulation of the Naringenin Pathway in the Presence of Perturbations

Comparison among the dynamic responses of the antithetic controller (solid line), direct controller (colored dashed line), and open-loop (black dashed line) for a malonyl-CoA perturbations of 60%. Time course variation in naringenin, CHS, and cellular growth (OD) for the three cases. Time course variation of the kaempferol response for both controllers. Time course variations of anti-σ and σ for the antithetic controller and cI for the direct controller. Perturbation occurs at t = 1 h. The gray area corresponds to the response before the perturbation is applied, and white area afterward. See also Figure S1 and Figure S2.

Figure 7 shows the predicted titers in naringenin production in open and closed loop obtained after 36 h. An initial titer close to 1 g L^{-1} of naringenin production is assumed in the engineered strain under optimal growth conditions. At time t = 1 h a perturbation occurs in the cell state leading to a decrease in the availability of the malonyl-CoA precursor. Such variability in malonyl-CoA intracellular concentration often occurs in environments where the cells are subjected to stress and environmental conditions are not uniform, as typically found in large fermenters. As expected, the depletion in a key metabolite critically impacted the naringenin pathway. For instance, a decrease of 40% in malonyl-CoA would lead to a decrease of about 25.0% in the concentration of naringenin. Such drop in production is, in turn, successfully attenuated by the closed-loop system, where the typical decrease in the naringenin titers is kept below 15.0%, a variation that is quite acceptable under industrial production conditions. Moreover, a 60% reduction in malonyl-CoA leads to a 40% drop in the production of naringenin, which can be attenuated up to around 25% in the closed-loop system. It is important to notice that these results were obtained for a set of parameters in the closed-loop system that were not optimized. Indeed, the results we obtained for the closed-loop regulation can be further improved by proper tuning of the controller and biosensor parameters. This is demonstrated by the fact that, in the case of malonyl-CoA decreasing down to a 60% of its nominal value, it is possible to keep the naringenin production over 96% of the nominal production for some values of parameters (see Supplemental Information).

Robustness of the Antithetic Integral Feedback Regulator and Comparison with the Direct Controller

In order to analyze the robustness of the circuit, we performed a sensitivity analysis modifying the model parameters for both the antithetic controller and the direct one. The values of the parameters were varied using the ranges listed in Table S3 at the Supplemental Information, based on typical values found in the literature.

For the antithetic controller, of the 2,911 possible combinations of parameters, 776 resulted in a naringenin production around the nominal level, 1 $\pm$ 0.05 g L^{-1} (Figure S3). Meanwhile, 15,700 combinations resulted

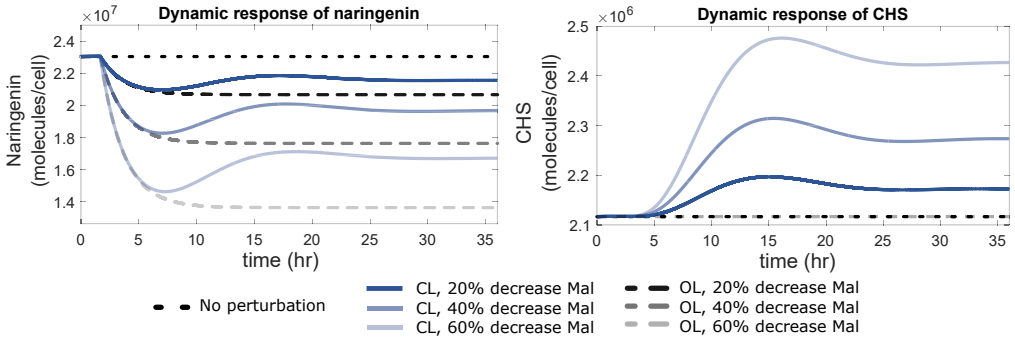

Figure 6. Comparison between Open-Loop and Closed-Loop Dynamic Responses for Malonyl-CoA Perturbations up to 60%

(A) Output response for naringenin concentration for a decrease in malonyl-CoA availability of 20%, 40%, and 60% in open and closed-loop.

(B) Time course variation in CHS concentration in the open-loop case (constant, no dynamic regulation) and the same changes in malonyl-CoA.

See also Figure S1.

in a production between 0.4 and 0.9 g L^{-1}, whereas the production levels for the remaining 565 combinations were found to be lower than 0.4 g L^{-1} (see Supplemental Information for further details on the Robustness analysis). In contrast, for the cI promoter direct controller, of the 2,193 combinations of parameters only 87 resulted in a naringenin production of 1 $\pm$ 0.05 g L^{-1}. Meanwhile, 507 combinations resulted in a production between 0.4 and 0.9 g L^{-1} and the remaining 1,599 combinations in a production lower than 0.4 g L^{-1}. Notice the parameters were varied between one and two orders of magnitude. In spite of such large variation, the antithetic controller successfully kept the output within the desired region of production in a region of parameters much broader than in the case of the direct controller. In addition, the antithetic controller demonstrates much less performance degradation, achieving a production over 0.4 g L^{-1} in more than 80% of the cases as compared with 27% cases with the direct controller.

What is found to be one of the most influential parameters of the biosensor and actuator was the plasmid copy number (Figure S4). To maintain the best performance (around 1 g L^{-1}) we found that the plasmid copy number of the biosensor ($C_{Na\sigma}$) must be 1 copy (250 solutions), 5 copies (230 solutions), or 10 copies (180 solutions). All together these three values represent more than 80% of the best solutions. With respect to the plasmid copy number of the actuator (C_{Nh}) the results were 5 copies (407 solutions) and 10 copies (387 solutions). All together these two values represent 100% of the best solutions (see Supplemental Information for further details).

DISCUSSION

Creating robust and stable microbial strains that produce large amounts of the target chemical for a long period at fermenter cultivation is a desirable industrial goal. Successful implementations of this goal need to start by finding suitable designs during the prototyping stage. Establishing feedback regulation in the pathway brings better stability and reproducibility during the process scaling-up. To that end, the selection of an appropriate biosensor in the feedback loop is necessary. Some biosensor-based proposals require the direct measurement of the metabolite of interest (Liu et al., 2015) or are based on sensing growth (Dinh et al., 2020). However, an issue at industrial production is the difficulty of measuring the concentration of the target metabolite or signal of interest through a biosensor because of their typically limited dynamic range, adapted to those levels found in natural environments. Therefore, adjusting the biosensor parameters remains challenging and a strategy that relies on model-based design has been recently proposed by Mannan et al. (2017). Here, we introduce an approach that combines the indirect measurement of the chemical target with an integral antithetic feedback controller, which has been demonstrated robust against environmental variability (Briat et al., 2016). A circuit called extended metabolic biosensor is introduced where a small amount of the chemical target is converted through several enzymatic steps into an effector for some given transcription factor. In order to minimize biosensor consumption, our strategy consists of engineering a production pathway that provides the nominal levels and an additional closed-loop circuit intended to regulate small fluctuations in the baseline pathway due to changing environmental conditions often found during the scaling-up.

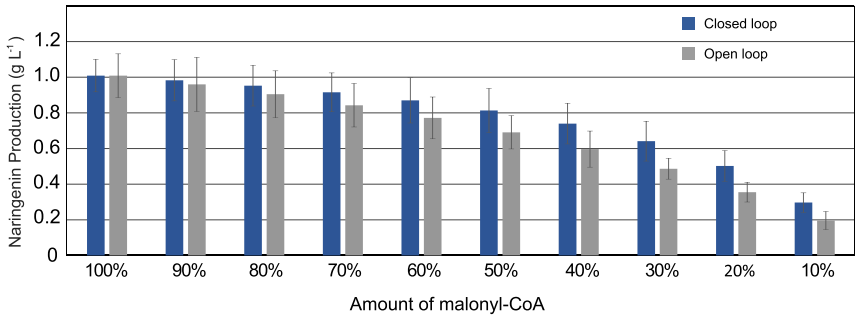

Figure 7. Naringenin Production Titers after 36 h under a Malonyl-CoA Perturbation in Open-loop Compared with the Closed-Loop Biosensor-Based Regulation

Error bars represent standard deviations due to parameter uncertainty.

This approach not only opens up new venues to achieve robust pathway regulation but also involves several challenges. Notably, the indirect measurement performed by the extended metabolic biosensor creates some unavoidable delay in the feedback loop that can lead to instabilities. As shown in this study, a careful design of the circuit parameters is necessary in order to ensure stability and robustness in the response.

Another innovation in the proposed feedback regulation approach is that the control circuit is performed at a mid-point in the pathway, i.e., in the expression of the CHS enzyme to counterbalance the perturbation coming from the malonyl-CoA availability. We have shown here that identifying the weakest step or the bottleneck in the pathway is essential in order to design a feedback regulation-based strain. Other regulation points in the pathway were possible, but choosing the regulation of expression of the CHS enzyme was the best choice because it was directly involved in the response to the malonyl-CoA perturbation. Regulating the expression of the four-gene naringenin pathway instead of the CHS gene could have been an alternative. However, this strategy would have led to overshooting and bumped behavior because of the weak link between malonyl-CoA availability and some of the enzymes and reactions involved in the pathway.

A promising improvement based on investigating the link between the availability of malonyl-CoA and growth involves expanding the proposed regulation genetic circuit. Since the malonyl-CoA precursor is mainly consumed in the cell in order to produce fatty acids that eventually will feed the cell for growth, sensing malonyl-CoA could be considered as a proxy for cell growth as well as other cell phenotypic traits. Therefore, widely used malonyl-CoA TF-based biosensors can provide the possibility of improving the proposed regulation by coupling production to cell growth.

Our control strategy involves a continuous and low-proportion (10^6:1) consumption of the target chemical through the extended metabolic biosensor in order to feed back the signal to the genetic controller. Tuning this metabolic pathway involves both reducing the affinity of the enzyme F3H to its substrate by a factor of 10^6 and reducing the catalytic activity by a factor of 60. In fact, these modifications are not an issue, as they entail a reduction in the enzymatic activity (Arnold, 2018).

As shown in this study, the integration of metabolic circuits and TF-based biosensors in pathway regulation is a robust solution for the high-performance production of target chemicals in the engineered microbial strains that are currently designed in modern biofoundries (Carbonell et al., 2018). Our analysis of the dynamic response of a cell factory under an extended metabolic biosensor circuit and antithetic feedback control has shown promising robust results against external and parametric perturbations compared with a direct controller, allowing a more efficient experimental design. Such devices are expected to become increasingly embedded as standard parts plugged into engineered strains for chemical production, enabling rapid prototyping and robust scale-up of microbial production from microplate prototypes to industrial levels.

Limitations of the Study

The present study analyzes an approach to synthetic pathway regulation based on indirect measurements and the use of an integral antithetic feedback control. In order to simulate the dynamic response of the system, we have focused on a study case for the production of the naringenin flavonoid and its enzyme

dynamics has been approximated through Michaelis-Menten kinetics. Kinetic constants were obtained from enzyme databases based on *in vitro* assays reported in the literature in order to define the value ranges of the parameters. We might expect actual values to differ, and for that reason a range was defined rather than constant values.

The study has focused on the main intermediates in the pathway, ignoring other effects such as co-factor availability as well as environmental conditions. Therefore, the study provides a first approximation to the problem that focuses on intrinsic properties rather than external factors, which were lumped on the single effect of the malonyl-CoA as the main external perturbation. As accurate whole-cell models for *E. Coli* become available (Goldberg et al., 2018), studies on dynamic pathway regulation will become more detailed and will allow for a larger set of environmental conditions and cell states to be tested. Future work includes extending the model to incorporate the malonyl-CoA dynamics and its relationship with the central metabolism and nutrients availability in the bioreactor. However, our current model does not include the metabolism of the cell and does not consider the possible implications in terms of genetic or metabolic burden. It has been shown that incorporating a genetic circuit in the cell can lead to metabolic burden reducing the overall performance of the cell (Ceroni et al., 2018). In this respect, we also foresee as future work the integration of the proposed strategy with whole-cell models (Nikolados et al., 2019) taking into account for the metabolic burden that the circuit and pathway incorporation add to the system. This will allow us, along with an optimization-based tuning of the circuit parameters (Boada et al., 2019, 2016), to seek for the set of parameters yielding the best naringenin production while introducing the minimal metabolic burden.

Similarly, the present study did not take into consideration challenges such as stability of the genetic circuit when expressed through a plasmid vector rather than through genome integration, especially in fermentation processes where the strains are under mechanical and chemical stress and fluctuations in the environmental conditions (Wehrs et al., 2019; Hicks et al., 2019). Inhibition effects of high producer strains might also be taken into account when analyzing the robustness of the circuit. The present study did not take into account stochastic fluctuations in enzyme abundance. However, it is becoming increasingly clear that expression variation may propagate to metabolites (Evans et al., 2020) leading to a negative impact production. It is expected that, in a stochastic scenario, our strategy including the antithetic controller would have a good performance (Briat et al., 2016). Finally, another limitation that challenges the application of the proposed approach is that it involves an invasive biosensor and therefore it is necessary to tune the circuit not only in order to obtain an appropriate dynamic range and response but also in order to keep a suitable conversion ratio of the product.

Resource Availability

Lead Contact

Further information and requests for resources should be directed to and will be fulfilled by the Lead Contact, Pablo Carbonell (pjcarbon@isa.upv.es).

Materials Availability

This study did not generate new unique reagents.

Data and Code Availability

Code for the models and simulations is available through GitHub (https://github.com/sb2cl/EMBA).

All the data obtained from the implemented mathematical model has been published as a Mendeley dataset (https://doi.org/10.17632/hpxhkyvctb.2).

METHODS

All methods can be found in the accompanying Transparent Methods supplemental file.

SUPPLEMENTAL INFORMATION

Supplemental Information can be found online at https://doi.org/10.1016/j.isci.2020.101305.

ACKNOWLEDGMENTS

This work is partially supported by grant MINECO/AEI and EU DPI2017-82896-C2-1-R. P.C. acknowledges support from the Universitat Politècnica de València Talento Programme.

AUTHORS CONTRIBUTIONS

P.C. and J.P. conceived the study. Y.B., A.V., J.P., and P.C. designed the experiments. Y.B and A.V. implemented the method and performed the experiments. P.C. wrote the initial version of the manuscript. Y.B., A.V., J.P., and P.C. edited and approved the final manuscript.

DECLARATION OF INTERESTS

The authors declare no competing interests.

Received: December 19, 2019
Revised: May 5, 2020
Accepted: June 18, 2020
Published: July 24, 2020

REFERENCES

Agrawal, D.K., Dolan, E.M., Hernandez, N.E., Blacklock, K.M., Khare, S.D., and Sontag, E.D. (2020). Mathematical models of protease-based enzymatic biosensors. ACS Synth. Biol. *9*, 198–208.

Aoki, S.K., Lillacci, G., Gupta, A., Baumschlager, A., Schweingruber, D., and Khammash, M. (2019). A universal biomolecular integral feedback controller for robust perfect adaptation. Nature *570*, 533–537.

Arnold, F.H. (2018). Directed evolution: bringing new chemistry to life. Angew. Chem. Int. Ed. *57*, 4143–4148.

Boada, Y., Reynoso-Meza, G., Picó, J., and Vignoni, A. (2016). Multi-objective optimization framework to obtain model-based guidelines for tuning biological synthetic devices: an adaptive network case. BMC Syst. Biol. *10*, 27.

Boada, Y., Vignoni, A., and Picó, J. (2017a). Engineered control of genetic variability reveals interplay among quorum sensing, feedback regulation, and biochemical noise. ACS Synth. Biol. *6*, 1903–1912.

Boada, Y., Vignoni, A., and Picó, J. (2017b). Multi-objective optimization for gene expression noise reduction in a synthetic gene circuit. IFAC-PapersOnLine *50*, 4472–4477.

Boada, Y., Vignoni, A., and Picó, J. (2019). Multiobjective identification of a feedback synthetic gene circuit. IEEE Trans. Control Syst. Technol. *28*, 208–223.

Briat, C., Gupta, A., and Khammash, M. (2016). Antithetic integral feedback ensures robust perfect adaptation in noisy bimolecular networks. Cell Syst. *2*, 15–26.

Briat, C., and Khammash, M. (2018). Perfect adaptation and optimal equilibrium productivity in a simple microbial biofuel metabolic pathway using dynamic integral control. ACS Synth. Biol. *7*, 419–431.

Carbonell, P., Jervis, A.J., Robinson, C.J., Yan, C., Dunstan, M., Swainston, N., Vinaixa, M., Hollywood, K.A., Currin, A., Rattray, N.J.W., et al. (2018). An automated design-build-test-learn pipeline for enhanced microbial production of fine chemicals. Commun. Biol. *1*, 66.

Carbonell, P., Parutto, P., Baudier, C., Junot, C., and Faulon, J.-L. (2014). Retropath: automated pipeline for embedded metabolic circuits. ACS Synth. Biol. *3*, 565–577.

Ceroni, F., Boo, A., Furini, S., Gorochowski, T.E., Borkowski, O., Ladak, Y.N., Awan, A.R., Gilbert, C., Stan, G.-B., and Ellis, T. (2018). Burden-driven feedback control of gene expression. Nat. Methods *15*, 387–393.

Chae, T.U., Choi, S.Y., Kim, J.W., Ko, Y.-S., and Lee, S.Y. (2017). Recent advances in systems metabolic engineering tools and strategies. Curr. Opin. Biotechnol. *47*, 67–82.

Chen, X., and Liu, L. (2018). Gene circuits for dynamically regulating metabolism. Trends Biotechnol. *36*, 751–754.

Cheng, F., Tang, X.-L., and Kardashliev, T. (2018). Transcription factor-based biosensors in high-throughput screening: advances and applications. Biotechnol. J. *13*, 1700648.

Choi, J.H., Keum, K.C., and Lee, S.Y. (2006). Production of recombinant proteins by high cell density culture of *Escherichia coli*. Chem. Eng. Sci. *61*, 876–885.

D'Ambrosio, V., and Jensen, M.K. (2017). Lighting up yeast cell factories by transcription factor-based biosensors. FEMS Yeast Res. *17*, fox076.

Delépine, B., Libis, V., Carbonell, P., and Faulon, J.-L. (2016). SensiPath: computer-aided design of sensing-enabling metabolic pathways. Nucleic Acids Res. *44*, W226–W231.

Dinh, C.V., Chen, X., and Prather, K.L.J. (2020). Development of a quorum-sensing based circuit for control of coculture population composition in a naringenin production system. ACS Synth. Biol. *9*, 590–597.

Doong, S.J., Gupta, A., and Prather, K.L.J. (2018). Layered dynamic regulation for improving metabolic pathway productivity in *Escherichia coli*. Proc. Natl. Acad. Sci. U S A *115*, 2964–2969.

Evans, C.R., Kempes, C.P., Price-Whelan, A., and Dietrich, L.E. (2020). Metabolic heterogeneity and cross-feeding in bacterial multicellular systems. Trends Microbiol.. https://www.sciencedirect.com/science/article/pii/S0966842X20300792

Gao, C., Xu, P., Ye, C., Chen, X., and Liu, L. (2019). Genetic circuit-assisted smart microbial engineering. Trends Microbiol. *27*, 1011–1024.

Goldberg, A.P., Szigeti, B., Chew, Y.H., Sekar, J.A., Roth, Y.D., and Karr, J.R. (2018). Emerging whole-cell modeling principles and methods. Curr. Opin. Biotechnol. *51*, 97–102.

Hicks, M., Bachmann, T.T., and Wang, B. (2019). Synthetic biology enables programmable cell-based biosensors. ChemPhysChem *21*, 132–144.

Hsiao, V., Swaminathan, A., and Murray, R.M. (2018). Control theory for synthetic biology: recent advances in system characterization, control design, and controller implementation for synthetic biology. IEEE Control Syst. *38*, 32–62.

Huyett, L.M., Dassau, E.J., Zisser, H.C., and Doyle, F. (2018). Glucose sensor dynamics and the artificial pancreas: the impact of lag on sensor measurement and controller performance. IEEE Control Syst. *38*, 30–46.

Johnson, A.O., Gonzalez-Villanueva, M., Wong, L., Steinbüchel, A., Tee, K.L., Xu, P., and Wong, T.S. (2017). Design and application of genetically-encoded malonyl-CoA biosensors for metabolic engineering of microbial cell factories. Metab. Eng. *44*, 253–264.

Juminaga, D., Baidoo, E.E.K., Redding-Johanson, A.M., Batth, T.S., Burd, H., Mukhopadhyay, A., Petzold, C.J., and Keasling, J.D. (2011). Modular engineering of l-tyrosine production in *Escherichia coli*. Appl. Environ. Microbiol. *78*, 89–98.

Koch, M., Pandi, A., Delépine, B., and Faulon, J.-L. (2018). A dataset of small molecules triggering transcriptional and translational cellular responses. Data Brief *17*, 1374–1378.

Leonard, E., Yan, Y., and Koffas, M.A. (2006). Functional expression of a P450 flavonoid hydroxylase for the biosynthesis of plant-specific hydroxylated flavonols in *Escherichia coli*. Metab. Eng. *8*, 172–181.

Lin, J.-L., Wagner, J.M., and Alper, H.S. (2017). Enabling tools for high-throughput detection of metabolites: metabolic engineering and directed evolution applications. Biotechnol. Adv. *35*, 950–970.

Liu, D., Mannan, A.A., Han, Y., Oyarzún, D.A., and Zhang, F. (2018). Dynamic metabolic control: towards precision engineering of metabolism. J. Ind. Microbiol. Biotechnol. *45*, 535–543.

Liu, D., Xiao, Y., Evans, B.S., and Zhang, F. (2015). Negative feedback regulation of fatty acid production based on a malonyl-CoA Sensor-Actuator. ACS Synth. Biol. *4*, 132–140.

Liu, D., and Zhang, F. (2018). Metabolic feedback circuits provide rapid control of metabolite dynamics. ACS Synth. Biol. *7*, 347–356.

Liu, L., Shan, S., Zhang, K., Ning, Z.-Q., Lu, X.-P., and Cheng, Y.-Y. (2008). Naringenin and hesperetin, two flavonoids derived from *Citrus aurantium* up-regulate transcription of adiponectin. Phytotherapy Res. *22*, 1400–1403.

Mahr, R., and Frunzke, J. (2015). Transcription factor-based biosensors in biotechnology: current state and future prospects. Appl. Microbiol. Biotechnol. *100*, 79–90.

Mannan, A.A., Liu, D., Zhang, F., and Oyarzún, D.A. (2017). Fundamental design principles for transcription-factor-based metabolite biosensors. ACS Synth. Biol. *6*, 1851–1859.

McKeague, M., Wong, R.S., and Smolke, C.D. (2016). Opportunities in the design and application of RNA for gene expression control. Nucleic Acids Res. *44*, 2987–2999.

Nielsen, A.A.K., Der, B.S., Shin, J., Vaidyanathan, P., Paralanov, V., Strychalski, E.A., Ross, D., Densmore, D., and Voigt, C.A. (2016). Genetic circuit design automation. Science *352*, aac7341.

Nikolados, E.-M., Weiße, A.Y., Ceroni, F., and Oyarzún, D.A. (2019). Growth defects and loss-of-function in synthetic gene circuits. ACS Synth. Biol. *8*, 1231–1240.

Paepe, B.D., Maertens, J., Vanholme, B., and Mey, M.D. (2018). Modularization and response curve engineering of a naringenin-responsive transcriptional biosensor. ACS Synth. Biol. *7*, 1303–1314.

Purdy, H.M., and Reed, J.L. (2017). Evaluating the capabilities of microbial chemical production using genome-scale metabolic models. Curr. Opin. Syst. Biol. *2*, 91–97.

Rahigude, A., Bhutada, P., Kaulaskar, S., Aswar, M., and Otari, K. (2012). Participation of antioxidant and cholinergic system in protective effect of naringenin against type-2 diabetes-induced memory dysfunction in rats. Neuroscience *226*, 62–72.

Rhodius, V.A., Segall-Shapiro, T.H., Sharon, B.D., Ghodasara, A., Orlova, E., Tabakh, H., Burkhardt, D.H., Clancy, K., Peterson, T.C., Gross, C.A., et al. (2013). Design of orthogonal genetic switches based on a crosstalk map of σs, anti-σs, and promoters. Mol. Syst. Biol. *9*, 702.

Rodriguez, A., Strucko, T., Stahlhut, S.G., Kristensen, M., Svenssen, D.K., Forster, J., Nielsen, J., and Borodina, I. (2017). Metabolic engineering of yeast for fermentative production of flavonoids. Bioresour. Technol. *245*, 1645–1654.

Segall-Shapiro, T.H., Sontag, E.D., and Voigt, C.A. (2018). Engineered promoters enable constant gene expression at any copy number in bacteria. Nat. Biotechnol. *36*, 352–358.

Shi, S., Ang, E.L., and Zhao, H. (2018). In vivo biosensors: mechanisms, development, and applications. J. Ind. Microbiol. Biotechnol. *45*, 491–516.

Shopera, T., He, L., Oyetunde, T., Tang, Y.J., and Moon, T.S. (2017). Decoupling resource-coupled gene expression in living cells. ACS Synth. Biol. *6*, 1596–1604.

Siedler, S., Stahlhut, S.G., Malla, S., Maury, J., and Neves, A.R. (2014). Novel biosensors based on flavonoid-responsive transcriptional regulators introduced into *Escherichia coli*. Metab. Eng. *21*, 2–8.

Snoek, T., Chaberski, E.K., Ambri, F., Kol, S., Bjørn, S.P., Pang, B., Barajas, J.F., Welner, D.H., Jensen, M.K., and Keasling, J.D. (2019). Evolution-guided engineering of small-molecule biosensors. Nucleic Acids Res. *48*, e3.

Stevens, J.T., and Carothers, J.M. (2015). Designing RNA-based genetic control systems for efficient production from engineered metabolic pathways. ACS Synth. Biol. *4*, 107–115.

Trantas, E., Panopoulos, N., and Ververidis, F. (2009). Metabolic engineering of the complete pathway leading to heterologous biosynthesis of various flavonoids and stilbenoids in *Saccharomyces cerevisiae*. Metab. Eng. *11*, 355–366.

Wang, R., Cress, B.F., Yang, Z., Hordines, J.C., Zhao, S., Jung, G.Y., Wang, Z., and Koffas, M.A.G. (2019). Design and characterization of biosensors for the screening of modular assembled naringenin biosynthetic library in *Saccharomyces cerevisiae*. ACS Synth. Biol. *8*, 2121–2130.

Wehrs, M., Tanjore, D., Eng, T., Lievense, J., Pray, T.R., and Mukhopadhyay, A. (2019). Engineering robust production microbes for large-scale cultivation. Trends Microbiol. *27*, 524–537.

Xu, P., Li, L., Zhang, F., Stephanopoulos, G., and Koffas, M. (2014). Improving fatty acids production by engineering dynamic pathway regulation and metabolic control. Proc. Natl. Acad. Sci. *111*, 11299–11304.

Xu, P., Ranganathan, S., Fowler, Z.L., Maranas, C.D., and Koffas, M.A. (2011). Genome-scale metabolic network modeling results in minimal interventions that cooperatively force carbon flux towards malonyl-CoA. Metab. Eng. *13*, 578–587.

Yang, Y., Lin, Y., Li, L., Linhardt, R.J., and Yan, Y. (2015). Regulating malonyl-CoA metabolism via synthetic antisense RNAs for enhanced biosynthesis of natural products. Metab. Eng. *29*, 217–226.

Zhou, S., Lyu, Y., Li, H., Koffas, M.A., and Zhou, J. (2019). Fine-tuning the (2 S)-naringenin synthetic pathway using an iterative high-throughput balancing strategy. Biotechnol. Bioeng. *116*, 1392–1404.

Zygmunt, K., Faubert, B., MacNeil, J., and Tsiani, E. (2010). Naringenin, a citrus flavonoid, increases muscle cell glucose uptake via AMPK. Biochem. Biophysical Res. Commun. *398*, 178–183.

iScience, Volume *23*

Supplemental Information

Extended Metabolic Biosensor Design for Dynamic Pathway Regulation of Cell Factories

Yadira Boada, Alejandro Vignoni, Jesús Picó, and Pablo Carbonell

Supplemental Information

Extended metabolic biosensor design for dynamic pathway regulation of cell factories

---

1. Transparent Methods

1.1. ***Metabolic pathway***

For every $i-$cell, the kinetics of the enzyme-catalyzed reactions involved in the metabolic pathway from L-tyrosine to naringenin (see Figure 2 in the main text) were modeled as the set of rate equations (1) obtained from mass balance equations and considering dilution due to cell growth rate μ.

$$\begin{aligned}
\frac{d[Lt]}{dt} &= V_0 - V_{Lt} - \mu[Lt] \\
\frac{d[pC]}{dt} &= V_{Lt} - V_{pC} - \mu[pC] \\
\frac{d[pA]}{dt} &= V_{pC} - V_{pA,Ma} - \mu[pA] \\
\frac{d[Nc]}{dt} &= V_{pA,Ma} - V_{Nc} - \mu[Nc] \\
\frac{d[N]}{dt} &= V_{Nc} - V_N - \mu[N]
\end{aligned} \tag{1}$$

For each reaction, V_j are the fluxes (molecules·min^{-1}). Lt is the number of molecules of L-tyrosine, pC is p-coumaric acid, pA is p-coumaroyl-CoA, Nc is naringenin chalcone, and N is naringenin, the flavonoid of interest. Ma is the number of molecules of malonyl-CoA, which is considered as a perturbation signal in the system.

We assume the flux V_0 corresponding to the precursor L-tyrosine keeps constant (see Table S1), and all fluxes V_j obey Michaelis-Menten kinetics (Michaelis and Menten, 1913) as follows:

$$\begin{aligned}
V_0 &= K_{Lt} \\
V_{Lt} &= \mathrm{k_{catTAL}}[TAL]\frac{[Lt]}{\mathrm{K_{mLt}} + [Lt]} \\
V_{pC} &= \mathrm{k_{cat4CL}}[4CL]\frac{[pC]}{\mathrm{K_{mpC}} + [pC]} \\
V_{pA} &= \mathrm{k_{catCHS}}[CHS]\frac{[pA][Ma]}{\mathrm{K_{mpA}\,K_{mMa}} + \mathrm{K_{mMa}}[pA] + \mathrm{K_{mpA}}[Ma] + [pA][Ma]} \\
V_{Nc} &= \mathrm{k_{catCHI}}[CHI]\frac{[Nc]}{\mathrm{K_{mNc}} + [Nc]} \\
V_N &= \mathrm{k_{catF3H}}[F3H]\frac{[N]}{\mathrm{K_{mN}} + [N]}
\end{aligned}$$

where $\mathrm{k_{catj}}$ is the catalytic rate of each enzyme (min^{-1}), and K_{mj} the Michaelis-Menten constant for each substrate. The enzyme kinetic parameters, detailed in Table S1, were obtained from Brenda (Schomburg et al., 2017).

Metabolic pathway			
Parameter	**Description**	**Value**	**Unit**
TAL	Enzyme amount	3.2e5	molec
4CL	Enzyme amount	6.48e5	molec
CHI	Enzyme amount	3.54e5	molec
F3H	Enzyme amount	2.81	molec
FLS	Enzyme amount	5.84	molec
CHS	Basal (open loop) enzyme amount	2.13e5	molec
K_{Lt}	L-tyrosine flux	2e6	molec $\cdot$ min^{-1}
M	Malonyl-CoA initial amount	2.34e4	molec
k_{catTAL}	TAL catalytic constant	1.2	min^{-1}
k_{cat4CL}	4CL catalytic constant	0.492	min^{-1}
k_{catCHS}	CHS catalytic constant	1.68	min^{-1}
k_{catCHI}	CHI catalytic constant	4.2	min^{-1}
k_{catF3H}	F3H catalytic constant	174	min^{-1}
k_{catFLS}	FLS catalytic constant	6	min^{-1}
K_{mLt}	Michaelis constant $\mathrm{TAL-Lt}$	1.9e4	molec
K_{mpC}	Michaelis constant $\mathrm{4CL-pC}$	1.4e4	molec
K_a	constant $\mathrm{CHS-M}$	1e-3	molec
K_b	constant $\mathrm{CHS-pC}$	1e-3	molec
K_{mNc}	Michaelis constant $\mathrm{CHI-Nc}$	2.8e4	molec
K_{mN}	Michaelis constant $\mathrm{F3H-N}$	5e8	molec
K_{mDi}	Michaelis constant $\mathrm{FHS-Di}$	1e4	molec

Table S1: Parameters for the metabolic pathway from L-tyrosine to kaempferol (Schomburg et al., 2017). Related to Figures 3 and 5.

The amounts of the enzymes TAL, 4CL, CHI and CHS corresponding to the pathway between L-tyrosine and naringenin were chosen so that the flux of precursor L-tyrosine can yield the targeted 1 g L^{-1} of naringenin (see Table S2).

Intracellular malonyl-CoA concentration is usually tightly regulated and maintained at very low levels in the cell (Yang et al., 2015). Therefore, for efficient production of malonyl-CoA derived molecules, enrichment of the intracellular malonyl-CoA pool is the standard practice. We considered a basal value of malonyl-CoA in the mid range of values reported in the literature (Wu et al., 2015; Takamura and Nomura, 1988; Xu et al., 2014). We avoid accumulation of large amounts of malonyl-CoA that may lead to growth inhibition.

1.2. ***Feedback regulation using the extended metabolic TF-based biosensor and the antithetic controller***

Next we model the feedback loop comprising the extended metabolic TF-based biosensor and the antithetic controller driving the co-expression of the enzyme CHS. Recall CHS is dynamically co-expressed through this feedback path in addition to its basal constant co-expression.

In this study, we focus on metabolic circuits that connect a target chemical to a transcription factor (TF)-based biosensor through their associated metabolic reactions. TF-based biosensors can be integrated as a genetic device into advanced sensing systems, defined here as TF-based extended metabolic biosensors, which consists of a proxy biosensor that detects changes in some target molecule by first transforming the molecule through one or several enzymatic steps into the effector molecule that drives the TF-based biosensor. Note that the target not necessarily has to be a single metabolite but is defined by a set of chemicals, which can correspond for instance to biomarkers or can be a proxy for biomass growth or other traits related to the strain phenotype and state. The extended biosensor space for a given target can be algorithmically mined through a metabolic expansion based on reaction rules (Delépine et al., 2016; Duigou et al., 2019). For an engineered production pathway involving n steps, each of the intermediates can be considered as targets for biosensors as well. Generally such intermediates are heterologous metabolites that do not interfere with other pathways in the host and therefore their detection through a biosensor can be used to probe different points in the engineered pathway.

Modeling TF-based extended biosensors requires the combination of the metabolic circuit transforming the target molecule T to the effector E and the TF-based biosensor. The dynamics of the circuit can be

approximated as the interconnection of two independent modules accounting for the metabolic circuit and the TF-based biosensor.

The metabolic circuit is typically modeled either using law mass action if concentrations of the enzymes are considered constant, or through Michaelis-Menten kinetics. We assume that gene expression of both the metabolic circuit and the biosensor is controlled by a single promoter (inducible or non-inducible).

The TF-based extended biosensor proposed in this work (Figure 2 in the manuscript) was modeled as follows.

1.2.1. Biosensor metabolic pathway stage

For every $i-$cell, and using the same assumptions as for the metabolic pathway between L-tyrosine and naringenin, the kinetics of the enzyme-catalyzed reactions involved in the metabolic pathway from naringenin to kaempferol (see Figure 2) were modeled as the set of rate equations (2):

$$\begin{aligned} \frac{d[Di]}{dt} &= V_N - V_{Di} - \mu[Di] \\ \frac{d[Ka]}{dt} &= V_{Di} - \mu[Ka] \end{aligned} \tag{2}$$

where V_j are the fluxes of each reaction (molecules·min^{-1}), Di is Dihydrokaempferol, and Ka is kaempferol, the effector flavonoid measured by the biosensor promoter. As for the pathway model (1), the flux V_{Di} obeys Michaelis-Menten kinetics:

$$V_{Di} = \mathrm{k_{catFLS}}[FLS]\frac{[Di]}{\mathrm{K_{mDi}} + [Di]}$$

The kinetic parameters, detailed in Table S1, were also obtained from Brenda (Schomburg et al., 2017). For the case of the enzymes involved in the extended metabolic biosensor we selected parameters from similar enzymes (eg. same product and different substrate). From the initial parameter range we tuned the values to achieve the desired gain for the biosensor. Directed evolution and statistical modeling can be used in order to experimentally tune the affinity and kinetics of the corresponding enzymes (Arnold, 2018; Berepiki et al., 2020).

1.2.2. Biosensor TF-based stage

Models describing the response of TF-based biosensors to changes in the effector concentration have been focused on determining the parameters of the dose-response curve, generally through a Hill function (Mannan et al., 2017; Trabelsi et al., 2018; Rogers et al., 2015, 2016). Performing a dose-response curve fitting is useful in order to determine static properties of the biosensor such as sensitivity, specificity or dynamic range, which are relevant for screening applications. However, employing a biosensor as part of a feedback circuit requires characterizing its dynamic response. Modeling the dynamics of TF-based biosensors has been less studied, with models either proposing apparent binding inhibition rate constants (with or without Hill's cooperativity) or data-driven models fitted to a linear system with delay.

Approaches to modeling the biosensor dynamics involve characterizing the time-dependent relationship between the input concentrations of the effector molecule and the target gene of interest through the dynamics of the biosensor internal states. Several dynamic models have been proposed in the literature. For instance, Zhang et al. (2012) developed a fatty acid/acyl-CoA biosensor based on the naturally occurring fatty acid-sensing protein FadR and its cognate regulator. The model for the biosensor in this study uses apparent rate constants for association and dissociation for FadR-ligand binding, as well as for association and dissociation of FadR-promoter complex. Gene expression, DNA replication and cell growth/species dilution are given by pseudo-first order rate constants. In another study, Feher et al. (2015) modeled the dynamic response of the malonyl-CoA biosensor considering production and dilution of the effector molecule and TF-binding to malonyl-CoA and promoter. The dynamic response was approximated to a second order linear system with a delay.

In our case, the TF-based stage of the biosensor uses the QdoR transcription factor, which represses the expression of the anti$-\sigma$ molecule by means of the qdoR-PqdoI promoter region (Siedler et al., 2014). The constitutive promoter J23106 (Anderson, accessed April 22, 2020) is used to express the QdoR transcription factor. Kaempferol captures the QdoR transcription factor, inactivating it. Equation (3) shows the resulting model for the dynamics of QdoR and anti$-\sigma$ as a function of QdoR and kaempferol.

$$\begin{aligned}
\frac{d[Q]^i}{dt} &= \frac{\mathrm{p_Q C_N k_Q}}{\mathrm{dm_Q} + \mu} - (\mathrm{d_Q} + \mu)\,[Q] \\
\frac{d[a\sigma]^i}{dt} &= \frac{\mathrm{p_{a\sigma} C_{N_{a\sigma}} k_{a\sigma}}}{\mathrm{dm_{a\sigma}} + \mu} \left(\alpha + \frac{(1-\alpha)\left(\mathrm{k_{dq} C_N}\right)^2 \left(\mathrm{k_{dk}} + [Ka]\right)^2}{\left(\mathrm{k_{dq} C_N}\right)^2 \left(\mathrm{k_{dk}} + [Ka]\right)^2 + \left(\mathrm{k_{dk}}[Q]\right)^2} \right) - \frac{\mathrm{k_{-c}}}{\mathrm{k_{dc}}}[\sigma][a\sigma] \\
&\quad + \mathrm{k_{-c}}[\sigma \cdot a\sigma] - (\mathrm{d_{a\sigma}} + \mu)\,[a\sigma]
\end{aligned} \tag{3}$$

where $a\sigma$ is the antifactor of σ protein, $\sigma \cdot a\sigma$ is the complex generated after σ sequestration (see section 1.2.3 below), Q is QdoR, and Ka is the amount of free kaempferol. All the parameters are listed in Table S1 and Table S2 .

To obtain the model (3), we considered the following assumptions for every i-cell:

- Transcription is fast enough as compared to translation, so it was assumed to be at quasi-steady state. Therefore, only the dynamics of proteins are considered.
- Translation is not a simple process (Alberts et al., 2009). It was modeled as an irreversible reaction with an average translation rate accounting for the fact that binding of ribosomes to the ribosome binding site (RBS) is indeed reversible, and several ribosomes may translate a single messenger RNA copy simultaneously.
- Degradation and dilution due to cells growth are considered for all species, including mRNA, with corresponding degradation rates $\mathrm{d_j}$ and specific growth rate μ.
- For each promoter, transcription activation or repression mediated by a transcription factor is modelled using a Hill-like function with the modification proposed in Trabelsi et al. (2018). This one accounts for the fact that the number of TFs and binding sites scale with the plasmid copy number.

1.2.3. Antithetic controller

Models based on ordinary differential equations for the antithetic feedback integral controller have been proposed in (Olsman et al., 2019; Aoki et al., 2019). In essence, the antithetic motif relies on the key mechanism of annihilation between the σ and anti$-\sigma$ factor and cofactor proteins. In our case, we considered the fact that the annihilation reaction, even though having a small dissociation constant, is reversible. As shown in Figure 2 from the manuscript, we considered production of the σ factor is induced by means of the dimer $(\mathrm{LuxR.AHL})_2$ using the PLux promoter. This way, the externally added amount of AHL acts as desired set-point for naringenin. Notice we do not assume the number of molecules of AHL needed to set a desired value for the ones of naringenin must be equal to this one – implying an unnecessary metabolic burden – but simply proportional. The free σ factor is a transcription factor for the promoter P20 used to express the naringenin chalcone synthase CHS, the output signal of the controller.

We considered the same assumptions as those used to derive the TF-based biosensor dynamics. The resulting model in equation (4) describes the dynamics of σ factor, the annihilation between σ and anti$-\sigma$,

and the production of CHS.

$$\begin{aligned}
\frac{d[\sigma]^i}{dt} &= \frac{\mathrm{p}_\sigma \mathrm{C_N} \mathrm{k}_\sigma}{\mathrm{dm}_\sigma + \mu}\left(\alpha + \frac{(1-\alpha)\,[A]^2}{\mathrm{k_{dlux}}\left(\frac{\mathrm{k_{d2}C_N}}{[R]}\right)^2 + [A]^2}\right) - \frac{\mathrm{k_{-c}}}{\mathrm{k_{dc}}}[\sigma][a\sigma] + \mathrm{k_{-c}}[\sigma \cdot a\sigma] - (\mathrm{d}_\sigma + \mu)\,[\sigma] \\
\frac{d[\sigma \cdot a\sigma]^i}{dt} &= \frac{\mathrm{k_{-c}}}{\mathrm{k_{dc}}}[\sigma][a\sigma] - \mathrm{k_{-c}}[\sigma \cdot a\sigma] - (\mathrm{d_c} + \mu)\,[\sigma \cdot a\sigma] \\
\frac{d[CHS]^i}{dt} &= \beta\frac{\mathrm{p_{H_c}C_N k_H}}{\mathrm{dm_H} + \mu} + \frac{\mathrm{p_H C_N k_H}}{\mathrm{dm_H} + \mu}\left(\alpha + \frac{(1-\alpha)\,[\sigma]^2}{\mathrm{k_{d20}}\left(\mathrm{k_{d\sigma}C_N}\right)^2 + [\sigma]^2}\right) - (\mathrm{d_H} + \mu)\,[CHS]
\end{aligned} \tag{4}$$

where A is the intracellular amount of AHL molecules (see below). All the parameters are listed in Table S2.

As mentioned above, we considered the desired set-point for naringenin is regulated by external addition of AHL, though indeed other extra- or intracellular signals could be used. In our case, we took into account that the interaction between AHL and AHL$_e$ represent the physical passive diffusion process for cell-to-cell communication via quorum sensing. This was modelled as a reversible pseudo-reaction using mass-action kinetics, resulting in the dynamics given by equation (5)

$$\begin{aligned}
\frac{d[R]^i}{dt} &= \frac{\mathrm{p_R C_N k_R}}{\mathrm{dm_R} + \mu} - (\mathrm{d_R} + \mu)\,[R] \\
\frac{d[A]^i}{dt} &= \mathrm{D}\,(\mathrm{V_c}[A_e] - [A]) - (\mathrm{d_A} + \mu)\,[A] \\
\frac{d[A_e]}{dt} &= \mathrm{D}\left(-x\mathrm{V_c}[A_e] + \sum_{i=1}^{x}[A]\right) - \mathrm{d_{Ae}}[A_e] \\
\frac{dx}{dt} &= \mu\left(1 - \frac{x}{\mathrm{x_{max}}}\right)x
\end{aligned} \tag{5}$$

where we also accounted for the dynamics of cell growth. R is LuxR protein; A and A_e are the intra and extracellular AHL molecules, respectively; and x is the number of cells in the culture. The term $\mathrm{V_c} = \frac{\mathrm{V_{cell}}}{\mathrm{V_{ext}}}$ is the ratio between the cellular and the environment volumes. As before, all the parameters are listed in Table S2.

1.3. ***Static regulation in open-loop***

In the open-loop production of naringenin, the enzyme CHS is expressed constitutively as shown in the schematic in Figure S1.

For the $i-$cell, the same assumptions described in Methods section *Biosensor TF-based stage* and *Antithetic controller* from the manuscript were taken to design the direct controller model. Equation (6) describes expression of CHS enzyme.

$$\frac{d[CHS]^i}{dt} = \frac{\mathrm{p_{H_c}C_N k_H}}{\mathrm{dm_H} + \mu} - (\mathrm{d_H} + \mu)\,[CHS] \tag{6}$$

Parameter $\mathrm{p}_{H_c} = 9.8239\,\mathrm{min}^{-1}$ was chosen to give the same level of expression than in the closed-loop configuration for a fair comparison. All the other parameters are the ones listed in Table S2.

1.4. ***Feedback regulation using a direct controller***

In the direct controller, cI protein replaces to σ and anti-σ cofactors from the antithetic controller as in Figure S2. The CHS enzyme is inhibited by the $lambda-$cI promoter region, when the TF-based biosensor detects an excess of naringenin and the subsequent kaempferol. This way, direct negative feedback regulates CHS expression, although reaching naringenin levels up to the 1 g L-1 set point is not guaranteed.

Biosensor and Antithetic controller gene circuit			
Parameter	**Description**	**Value**	**Unit**
μ	specific growth rate	$8.5e{-3}$	min^{-1}
α	tight basal expression	0.01	adim
β	constitutive expression	1.5	adim
C_N, $\text{C}_{\text{Na}\sigma}$	Plasmid copy number	10	copies
D	AHL diffusion rate across cell membrane	2	min^{-1}
k_σ, $\text{k}_\text{a}\sigma$	transcription rate	1.98	min^{-1}
k_R	transcription rate	0.78	min^{-1}
k_H	transcription rate	3.67	min^{-1}
k_Q	transcription rate	0.71	min^{-1}
p_σ	translation rate	3	min^{-1}
$\text{p}_{\text{a}\sigma}$	translation rate	3.17	min^{-1}
p_R	translation rate	2.34	min^{-1}
p_H	translation rate	92.4	min^{-1}
p_Hc	constitutive translation rate	$6.5e{-4}$	min^{-1}
p_Q	translation rate	2.55	min^{-1}
d_R	protein degradation rate	0.02	min^{-1}
d_c	degradation rate $[\sigma \cdot a\sigma]$	$1e{-3}$	min^{-1}
d_A	Intracellular degradation rate	$4e{-4}$	min^{-1}
d_Ae	Extra cellular degradation rate	$4.8e{-5}$	min^{-1}
kd_{20}	dissociation constant to p_{20}	1000	molec
kd_lux	dissociation constant to p_{lux}	600	molec
kd_σ	dissociation constant σ dimer	1000	molec
kd_q	dissociation constant to p_{qdoI}	150	molec
kd_k	dissociation constant QdoR to kaempferol	75	molec
kd_c	dissociation constant $[\sigma \cdot a\sigma]$	0.01	molec
$\text{kd}_{-\text{c}}$	dissociation rate $[\sigma \cdot a\sigma]$	0.018	min^{-1}
k_c	association rate $(\sigma \cdot a\sigma)$	1.8	min^{-1}
dm_σ, $\text{dm}_{\text{a}\sigma}$, dm_R, dm_H, dm_Q	mRNA degradation rate	0.231	min^{-1}
d_σ, $\text{d}_{\text{a}\sigma}$, d_H, d_Q	protein degradation rate	$3e{-4}$	min^{-1}
Comparison with cI direct controller gene circuit			
$\text{kd}_{\lambda\text{cI}}$	dissociation constant to $\text{p}_{\lambda\text{cI}}$	1000	molec
$\text{C}_{\text{N}_\text{cI}}$	Plasmid copy number	10	copies
p_hcI	translation rate	54.89	min^{-1}
p_cI	translation rate	3.17	min^{-1}

Table S2: Gene circuit parameters were taken from (Boada et al., 2017; Annunziata et al., 2017) and (Siedler et al., 2014). Related to Figures 3 and 5.

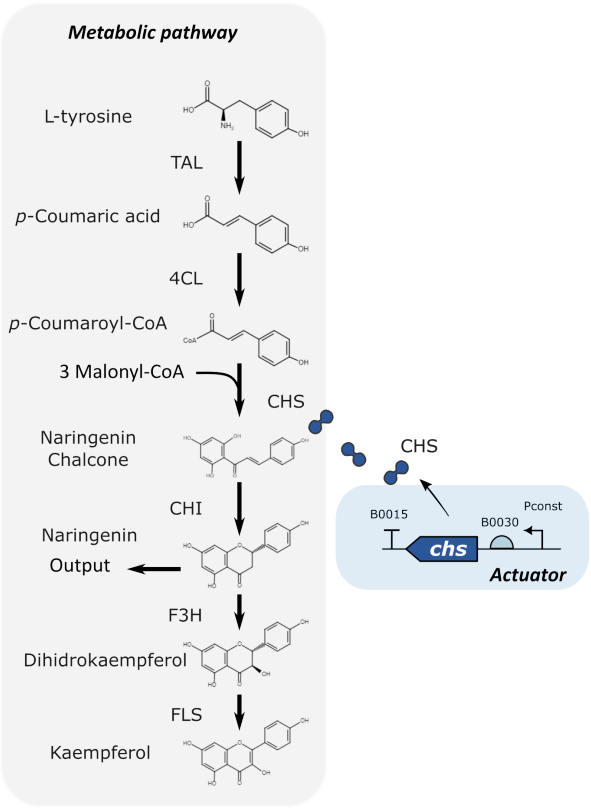

Figure S1: Open-loop configuration. Schematic of the naringerin biosynthesis pathway with constitutive CHS enzyme expression. Related to Figures 5 and 6.

For the $i-$cell, the same assumptions described in sections *Biosensor TF-based stage* and *Antithetic controller* from the manuscript were taken to design the direct controller model. Equation (7) describes the cI protein expression when the naringenin and kaempferol amount increased. Then, cI will repress the CHS production as in equation (8) until naringenin chalcone decreases. cI has a similar temporal dynamics of anti-σ.

$$\frac{d[cI]^i}{dt} = \frac{\mathrm{p_{cI}C_{N_{cI}}k_{cI}}}{\mathrm{dm_{cI}}+\mu}\left(\alpha + \frac{(1-\alpha)\left(\mathrm{k_{dq}C_N}\right)^2\left(\mathrm{k_{dk}}+[Ka]\right)^2}{\left(\mathrm{k_{dq}C_N}\right)^2\left(\mathrm{k_{dk}}+[Ka]\right)^2+\left(\mathrm{k_{dk}}[Q]\right)^2}\right) - \left(\mathrm{d_{cI}}+\mu\right)[cI] \tag{7}$$

$$\frac{d[CHS]^i}{dt} = \frac{\mathrm{p_{H_c}C_Nk_H}}{\mathrm{dm_H}+\mu} + \frac{\mathrm{p_HC_Nk_H}}{\mathrm{dm_H}+\mu}\left(\alpha + \frac{(1-\alpha)\,[cI]^2}{\mathrm{k_{d20}}\left(\mathrm{k_{dcI}C_N}\right)^2+[cI]^2}\right) - \left(\mathrm{d_H}+\mu\right)[CHS] \tag{8}$$

where cI is the cI protein, Q is QdoR, and Ka is the amount of free kaempferol. All the parameters are listed in Table 2 from the main text. Equations for QdoR production and for the naringerin metabolic pathway remain the same.

1.5. ***Robustness analysis***

In order to study how the different strategies respond to a variation on the values of the parameters, we selected the following parameters and ranges enumerated in Table S3.

For each parameter combination we obtain the naringenin production level without perturbation and with a 60% reduction in the available amount of malonyl-CoA. We performed this analysis for both the

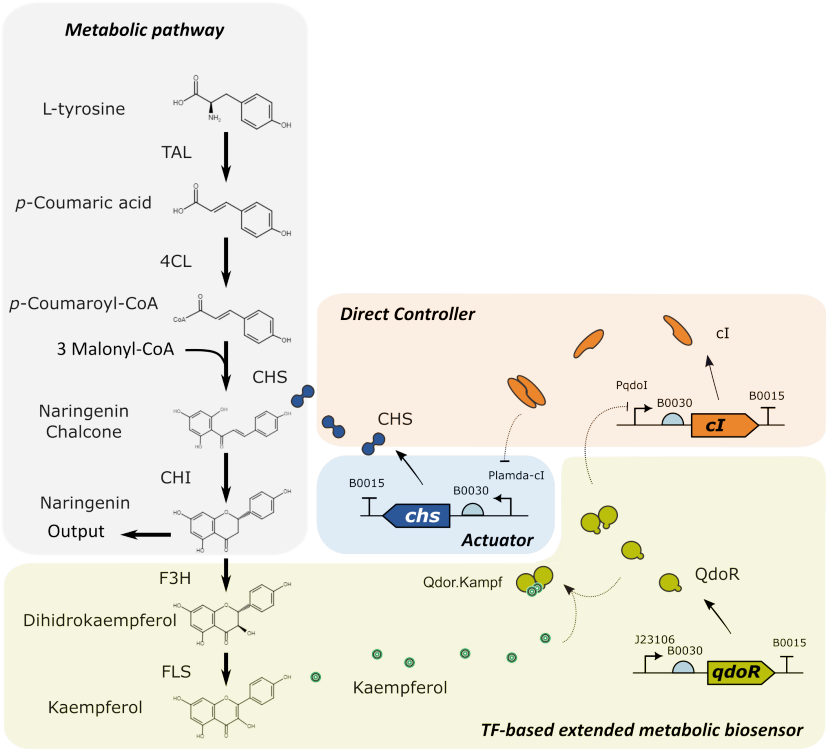

Figure S2: Direct feedback controller. Schematic of the naringerin biosynthesis pathway, where cI protein regulates CHS enzyme production. Related to Figure 5.

Robustness analysis			
Parameter	**Range**	**Nominal Value**	**Unit**
kd_{20}, $\mathrm{kd}_{\mathrm{lamcI}}$	$[250, 5500]$	1000	molec
kd_{q}	$[1, 500]$	150	molec
$\mathrm{CN}_{\mathrm{a}\sigma}$, $\mathrm{CN}_{\mathrm{cI}}$	$[1, 100]$	10	copies
$\mathrm{CN}_{\mathrm{CHS}}$	$[1, 100]$	10	copies
$\mathrm{p}_{\mathrm{a}\sigma}$, p_{cI}	$[0.5, 10]$	3.17	min^{-1}
p_{h}	$[1, 20]$	15.62	min^{-1}
$\mathrm{p}_{\mathrm{hcI}}$	$[3.5, 70]$	54.3	min^{-1}

Table S3: Range for the selected parameters. Related to Figure 2.

antithetic controller and the direct controller. The results are shown in Figure S3. There in the horizontal axis is depicted the level of naringenin production for each combination. In the vertical axis we plot the naringenin production with the perturbation relative to the unperturbed production. In this way, a point with 1 g L^{-1} in the horizontal axis and a 100% in the vertical would have the same level of production without and with the perturbation, note this would be an ideal situation.

As it is possible to see, the antithetic controller has more solutions in the upper part of the naringenin production (x-axis) than the direct controller. In a tuning stage it would be possible to select the parameters of the antithetic controller, corresponding to one of the solutions keeping large production values even under perturbations. Therefore, this controller will have a very good performance. In contrast, the direct controller has a big portion of its solutions grouped in the low producing end of the plot (low x-axis values), having an additional upper limit for the naringenin production with perturbation of 90%.

In Figure S4 we show the distribution of parameter values for the solutions with good performance

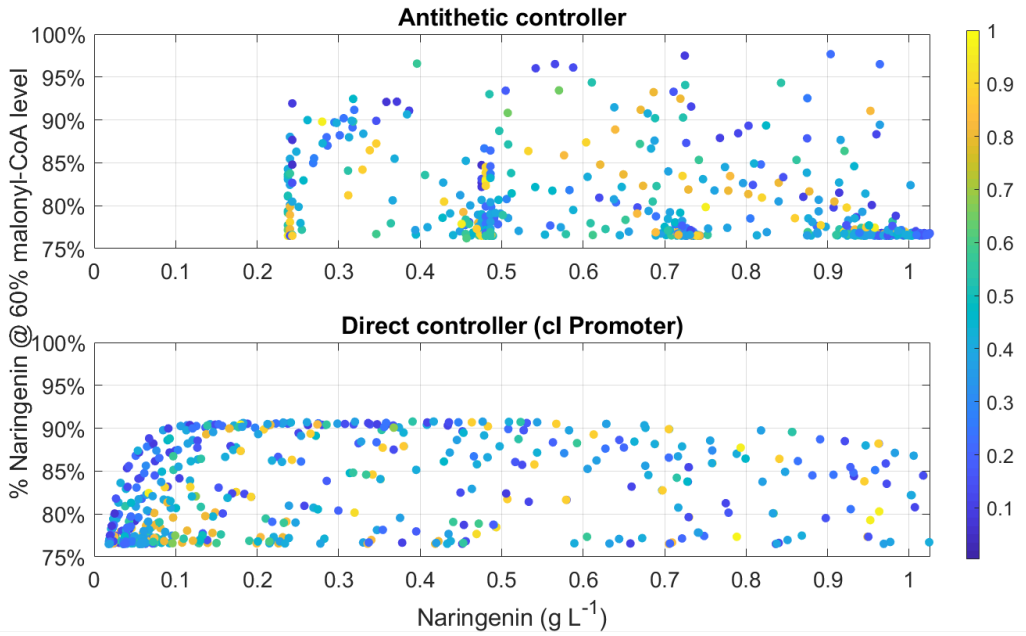

Figure S3: Performance comparison between the antithetic controller and the direct controller. The dots represent the production of certain parameter combination. The color of the dots, represent the distance to the nominal point (i.e. the one used in the main body of the paper for all the simulations giving a production of 1 g L^{-1}) where blue means short distance and yellow means big distance. Related to Figure 5.

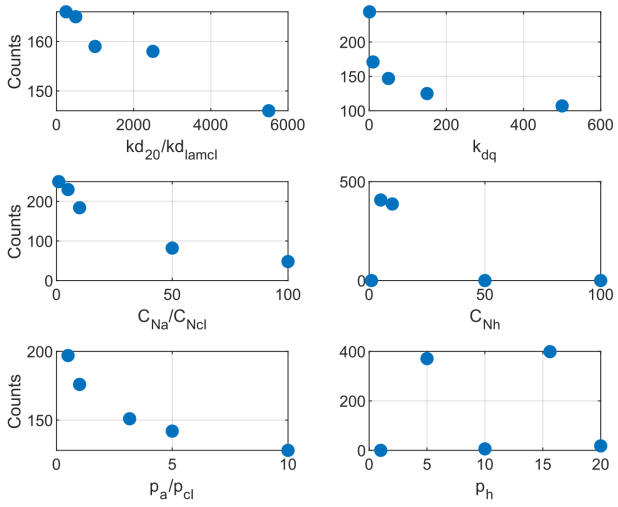

Figure S4: Number of solutions with good performance for each parameter value. Related to Figure 2.

(around 1 g L^{-1}) to see which parameter has a bigger influence. Here, we found that the copy number associated with most of the solutions with good performance are in the following ranges:

- The copy number of the plasmid of the biosensor (the one with the Pqdol promoter driving the expression of Anti$-\sigma$) 1 plasmid (250 solutions), 5 plasmids (230 solutions) and 10 plasmids (180

solutions). All together these three values represent more than 80% of the good solutions.

- The copy number of the plasmid of the actuator (the one with the P20 promoter driving the expression of CHS) 5 plasmid (407 solutions) and 10 plasmids (387 solutions). All together these two values represent 100% of the good solutions.

Supplemental References

Alberts, B., Bray, D., Hopkin, K., Johnson, A. D., Johnson, A., Roberts, K., Lewis, J., Raff, M., and Walter, P. (2009). *Essential Cell Biology*. (3rd ed.). Garland Science.

Anderson, J. C. (accessed April 22, 2020). Anderson promoter collection. MIT: Registry of Standard Biological Parts. `http://parts.igem.org/Promoters/Catalog/Anderson`.

Annunziata, F., Matyjaszkiewicz, A., Fiore, G., Grierson, C. S., Marucci, L., di Bernardo, M., and Savery, N. J. (2017). An orthogonal multi-input integration system to control gene expression in escherichia coli. *ACS Synthetic Biology*, *6*, 1816–1824.

Duigou, T., du Lac, M., Carbonell, P., and Faulon, J.-L. (2019). RetroRules: a database of reaction rules for engineering biology. *Nucleic Acids Research*, *47*, D1229–D1235.

Feher, T., Libis, V., Carbonell, P., and Faulon, J.-L. (2015). A Sense of Balance: Experimental Investigation and Modeling of a Malonyl-CoA Sensor in Escherichia coli. *Frontiers in Bioengineering and Biotechnology*, *3*, 46.

Michaelis, L., and Menten, M. (1913). Die kinetik der invertinwirkung biochem z 49: 333–369. *Find this article online*, .

Olsman, N., Baetica, A.-A., Xiao, F., Leong, Y. P., Murray, R. M., and Doyle, J. C. (2019). Hard Limits and Performance Tradeoffs in a Class of Antithetic Integral Feedback Networks. *Cell Systems*, *9*, 49–63.e16.

Rogers, J. K., Guzman, C. D., Taylor, N. D., Raman, S., Anderson, K., and Church, G. M. (2015). Synthetic biosensors for precise gene control and real-time monitoring of metabolites. *Nucleic Acids Research*, *43*, 7648–7660.

Rogers, J. K., Taylor, N. D., and Church, G. M. (2016). Biosensor-based engineering of biosynthetic pathways. *Current Opinion in Biotechnology*, *42*, 84–91.

Schomburg, I., Jeske, L., Ulbrich, M., Placzek, S., Chang, A., and Schomburg, D. (2017). The BRENDA enzyme information system–From a database to an expert system. *Journal of Biotechnology*, *261*, 194–206.

Takamura, Y., and Nomura, G. (1988). Changes in the intracellular concentration of acetyl-CoA and malonyl-CoA in relation to the carbon and energy metabolism of escherichia coli k12. *Microbiology*, *134*, 2249–2253.

Trabelsi, H., Koch, M., and Faulon, J.-L. (2018). Building a minimal and generalizable model of transcription factor–based biosensors: Showcasing flavonoids. *Biotechnology and Bioengineering*, *115*, 2292–2304.

Wu, J., Du, G., Chen, J., and Zhou, J. (2015). Enhancing flavonoid production by systematically tuning the central metabolic pathways based on a CRISPR interference system in escherichia coli. *Scientific Reports*, *5*.

Zhang, F., Carothers, J. M., and Keasling, J. D. (2012). Design of a dynamic sensor-regulator system for production of chemicals and fuels derived from fatty acids. *Nature Biotechnology*, *30*, 354–359.